ORIGINAL ARTICLE

lajss.org© Latin American Journal of Solids and Structures

www.lajss.org

Experimental and numerical simulation analysis of the dynamic characteristics of a new piezoelectric friction damper

Jianbo Dai[a]*, Zewen Zhao[b], Hao Wang[c], Jing Ma[d], Xuhao Liang[e]

[a] School of Civil Engineering, Xi'an Shiyou University, Xi'an 710065, China. Email: d_jianbo@foxmail.com
[b] School of Mechanical Engineering, Xi'an Shiyou University, Xi'an 710065, China. E-mail: zzw15682993428@163.com
[c] School of Mechanical Engineering, Xi'an Shiyou University, Xi'an 710065, China. E-mail: 1553282108@qq.com
[d] School of Mechanical Engineering, Xi'an Shiyou University, Xi'an 710065, China. E-mail: 2501048207@qq.com
[e] School of Mechanical Engineering, Xi'an Shiyou University, Xi'an 710065, China. E-mail: 644061140@qq.com

* Corresponding author

https://doi.org/10.1590/1679-78257902

Abstract

Based on the inverse piezoelectric effect and other characteristics of piezoelectric ceramics, a new type of piezoelectric variable friction damper is developed, and the output performance test of piezoelectric ceramic actuator and piezoelectric variable friction damper is carried out, and the parametric mechanical model of the damper is established by using Simulink to carry out numerical simulation, and compared and analyzed with the test results. The results of the study show that the simulation and the test present a good regular agreement. With the increment of loading voltage, the displacement deformation and zero-displacement thrust of piezoelectric ceramic actuator are approximately linear with the loading voltage; when the loading voltage is increased by 15V every time, the test value of the output damping force of the damper increases by 259.66N on average step by step, and the simulated value increases by 256.14N step by step, and the damping force has a linearly incremental relationship with the voltage and the slope of the linear increase is 16.434.

Keywords

Piezoelectric Variable Friction Damper; Piezoelectric Ceramics; Output Performance; Damping Force; Applied Voltage.

Graphical Abstract

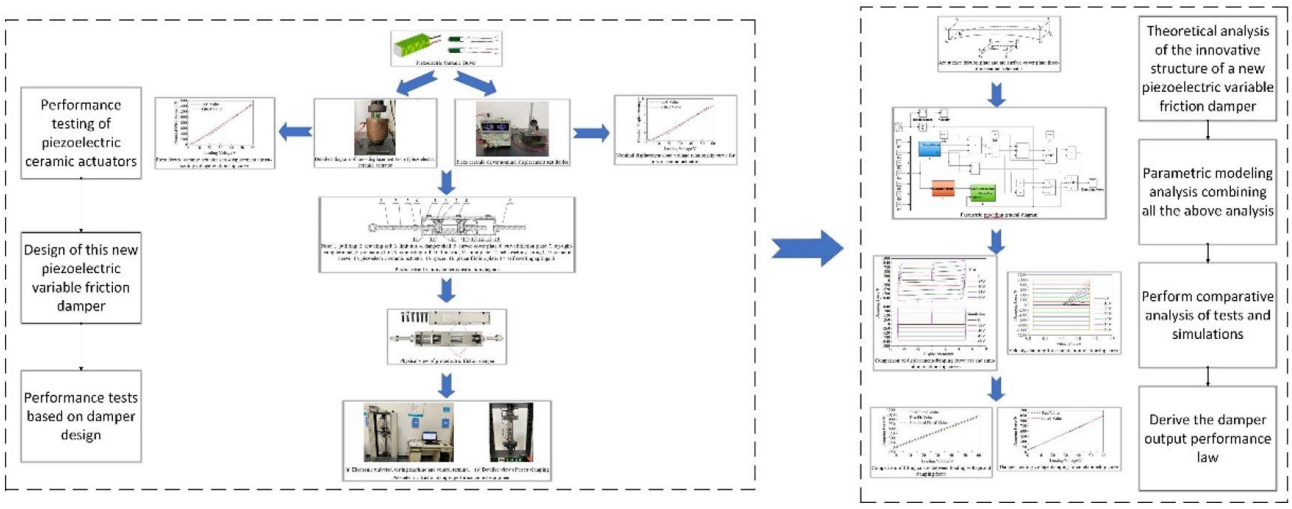

Received: November 04, 2023; In revised form: November 09, 2023; Accepted: November 20, 2023; Available online: November 28, 2023.
https://doi.org/10.1590/1679-78257902

1 INTRODUCTION

Energy dissipation and vibration reduction technology is an effective way to improve structural vibration resistance and realize vibration control (Liu, 2022). Friction dampers have been widely used due to the advantages of low cost and high energy dissipation capacity (López et al, 2004). However, traditional friction dampers have the following drawbacks in use: the dampers provide a constant friction force, which cannot meet the energy dissipation needs of different seismic responses; the dampers do not have the ability of self-resetting, which makes the structural residual deformation larger and difficult to repair (Qu, et al, 2023 and Jaisee et al, 2021). In view of this, this paper designs and develops a new type of piezoelectric variable friction damper, and carries out experimental and simulation studies on the output performance of the damper to ensure that the piezoelectric variable friction damper can be operated safely and has engineering application value.

Piezoelectric ceramics, as a new type of smart material, has the advantages of piezoelectric effect, high sensitivity, wide frequency range, fast response, high temperature resistance, and tunability (Yao et al, 2019), which makes piezoelectric ceramics have unique advantages in the field of vibration control. Li et al (2023) proposed a composite control method to improve the positioning accuracy of piezoelectric ceramic actuators with respect to the hysteresis nonlinear characteristic in piezoelectric ceramic actuators. Padoin et al (2015) and others used a linear quadratic regulator (LQR)--based control strategy aimed at optimizing the installation location of piezoelectric actuators in laminated composite structures to maximize their structural vibration control. Sokół (2020) used the inverse piezoelectric effect of piezoelectric ceramic elements to study slender systems in terms of vibration frequency and load capacity, integrating piezoelectric ceramic materials with the host structure to create configurations capable of adapting to different conditions. Sun et al (2017) used piezoelectric ceramics as an actuator/sensor for the first time and employed a multi-modal fuzzy sliding mode controller to suppress the vibration of a conical-shell structure. A modal analysis was carried out on the structure using the finite-element method to get the intrinsic frequency and vibration pattern of the structure, which was verified by modal tests. Piezoelectric variable friction dampers utilize the piezoelectric effect of piezoelectric ceramic materials to achieve vibration energy dissipation by the interaction between their mechanical structures, so the unique properties of this type of dampers have become the research direction of many scholars in vibration control and energy dissipation. Dai et al (2013) developed a new piezoelectric variable friction damp-er that can provide adjustable friction damping force in either horizontal direction using a commercial standard laminated piezoelectric actuator and a circular friction disk, which can work with a circular vibration isolation pad to form an intelligent vibration isolation system. Zhu et al (2017) proposed a new criterion for determining the dynamic stability of rod system structures. The criterion is based on the energy method and utilizes a variety of parameters from an independently researched piezoelectric variable friction damper, which is applied to the structural system. Zhan et al (2015) designed a piezoelectric friction damper with a reset function, and proposed two damper mounting methods according to the structural force and deformation characteristics of the transmission tower model. Wang et al (2021) designed and fabricated a novel piezoelectric ceramic friction damper based on the piezoelectric effect of piezoelectric ceramics. Cyclic load tests were performed to determine the selection of friction discs for the PCFD, and hysteresis performance tests were performed to evaluate the energy dissipation capacity of the PCFD at different voltages was evaluated, and the semi-active control under seismic excitation was simulated using Simulink for a three-layer frame structure model. Zhang et al (2023) proposed a novel piezoelectric variable friction damper. The mechanical model of the PFD and the effects of loading speed, displacement amplitude, voltage, friction plate material, piezoelectric stack actuator size and spring parameters on the hysteresis characteristics of the PFD were investigated through experiments and numerical simulations.

Based on the above research findings, the piezoelectric variable friction damper and its application is a research hotspot in recent years, but the structural design of piezoelectric variable friction damper and the study of the dynamic characteristics still has a large optimization space, which requires further analysis and experimental verification. This paper combines the characteristics of piezoelectric ceramics and friction dampers, designs and develops a new type of piezoelectric variable friction damper, carries out the dynamic characteristic test of piezoelectric variable friction damper, and explores the dynamic characteristic law of the damper.

2 PIEZO CERAMIC DRIVER OUTPUT PERFORMANCE TEST

2.1 Driver Constitutive Equations and Performance Parameters

Piezoelectric materials can realize the mutual conversion of electrical and mechanical energy and have good electromechanical coupling properties. Its constitutive equation (Ou and Yang, 2003) can be expressed as:

$$\varepsilon = c^E \sigma + dE \tag{1}$$

$$D = d\sigma + \varepsilon^\sigma E \tag{2}$$

where ε is the piezoelectric material strain, c^E is the elastic flexibility coefficient, σ is the piezoelectric material stress, d is the piezoelectric strain constant, E is the applied electric field strength, D is the potential shift, and ε^σ is the dielectric constant.

From equation (1) and equation (2), the total strain of the piezoelectric material consists of the sum of the strain generated by the applied electric field strength and the strain generated by the applied stress, and the strain and the potential shift of the piezoelectric material vary with the applied electric field strength and the stress, respectively.

The developed piezoelectric variable friction damper uses a piezoelectric ceramic actuator consisting of a stack of 180 piezoelectric ceramic monoliths bonded by epoxy resin, model BCS3-101018, with displacements of up to 20 μm. The package diagram and the physical figure are shown in figure 1, and the main performance parameters are shown in Table 1.

Figure 1 Piezoelectric Ceramic Driver

Table 1 Main performance parameters of piezoelectric ceramic driver

External dimension *A*×*B*×*H* [mm]	Nominal displacement [*μm*@150V](±15%)	Zero-displacement thrust [*N*@150V]	Stiffness [*N*/*μm*]	Electrostatic capacity [*μF*] (±15%)	Resonant frequency [kHz]
10×10×18	20	4000	200	6.0	65

2.2 Driver Output Performance Testing and Analysis

The test utilizes a digital micrometer to determine the nominal displacement size and zero-displacement thrust size of the piezoelectric ceramic actuator in the mechanically free and mechanically clamped states, respectively, to verify the accuracy of its main performance parameters and the reasonableness of the selection of this type of piezoelectric stack. The test selected 0~60V DC constant voltage, according to 0V,10V,20V,30V,40V,50V,60V loaded to the positive and negative extremes of piezoelectric ceramic driver.

(1)Nominal Displacement Test

The nominal displacement of the piezoelectric ceramic actuator is tested by placing the piezoelectric ceramic actuator vertically under the probe of the digital micrometer and zeroing the micrometer to balance the effect of its own gravity, and connecting the energized DC regulated power supply through the wires. Before the start of the test, the applied voltage was adjusted to the required size, and after the start of the test, the changes in the digital micrometer were observed and recorded. The test setup is shown in figure 2.

Figure 3 shows the nominal displacement of piezoelectric ceramic actuator - loading voltage test and fitting curve. From the figure, the voltage between 20V ~ 30V curve slope is the largest, compared with the voltage of 0 ~ 20V displacement growth rate increased by 50%, the reason may be that the voltage loading piezoelectric ceramic actuator under the polarization reaction is more intense, so the displacement response is the most sensitive, but displacement basically shows a linear increase. The overall trend of the curve shows that the displacement and deformation of the piezoelectric ceramic actuator increases with the loading voltage, and the size of the loading voltage is approximately linear relationship. The curve is fitted by MATLAB, and the linear relationship between the loading voltage and the nominal displacement with an approximate slope of 0.1482 can be obtained:

$$D = 0.1482U - 0.5607 \tag{3}$$

In Equation (3), D is the nominal displacement and U is the loading voltage.

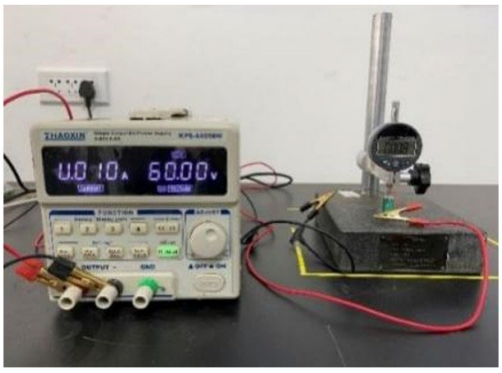

Figure 2 Piezo ceramic driver nominal displacement test device

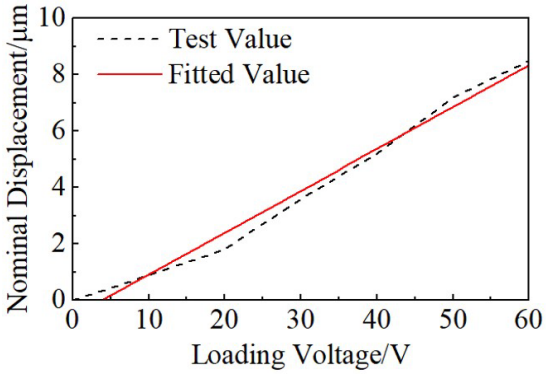

Figure 3 Nominal displacement-load voltage relationship curve for piezo ceramic actuators

(2)Zero-displacement Thrust Test

The zero-displacement thrust size of the piezoelectric ceramic actuator is tested by clamping the piezoelectric ceramic actuator vertically and vertically using a microcomputer-controlled electronic universal testing machine and connecting a good DC regulated power supply. Before the test starts, a certain amount of pre-pressure needs to be applied using the computer control system, and after the test starts, the size of the zero-displacement thrust under different loading voltages displayed at the control terminal is observed and recorded. The test setup is shown in figure 4.

Figure 4 Detailed diagram of zero displacement test of piezoelectric ceramic actuator

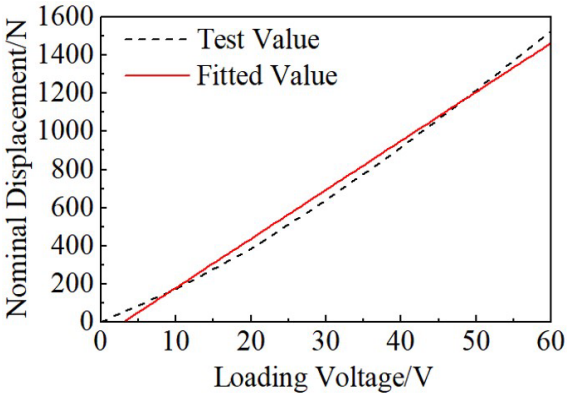

Figure 5 Piezoelectric ceramic actuator zero-displacement thrust-loading voltage relationship curve

Figure 5 shows the zero-displacement thrust-loading voltage test and fitting curves of the piezoelectric ceramic actuator. From the figure, when the voltage is 10V, 30V, and 60V, the thrust force is 172.8N, 640N, and 1529.6N, respectively, which indicates that the zero-displacement thrust force of the piezoelectric ceramic actuator increases with the voltage under the mechanical clamping, and shows a strong linear relationship. The curve was fitted by MATLAB to obtain a linear relationship between loading voltage and zero-displacement thrust with a slope of 25.7371:

$$F = 25.7371U - 78.1714 \tag{4}$$

In Equation (4), F is the zero-displacement thrust and U is the loading voltage.

3 DEVELOPMENT AND EXPERIMENTAL ANALYSIS OF PIEZOELECTRIC VARIABLE FRICTION DAMPERS

3.1 Design of the Damper

The basic structure of the piezoelectric variable friction damper designed in this paper is shown in figure 6, and the physical drawing is shown in figure 7. The overall shell length of the damper is set to 190mm, and the length of the limit rod is set to 56mm, which can make the displacement stroke of the actuator rod controlled at about 10mm. The test of adjusting the size of the preloading bolt (8) shows that the piezoelectric ceramic actuator (14) maintains the mechanical clamping state when a single bolt maintains a preload force of 200N~260N. At this time, in the voltage excitation driver will produce zero-displacement thrust, so that in the upper part of the damper can produce curved cover plate (5) and curved friction plate (6) interaction force, the bottom can produce the damper shell (4) and planar friction plate (16) interaction force. At this time, if there is external interference, it will pull the actuating rod (2) to the left or right movement through the pull ring (1), so that the two piezoelectric ceramic actuators as a whole synchronized movement, to achieve a strong friction damping force in the interior of the damper. After the damper is powered off, under the action of the self-resetting springs (12),(17), the piezoelectric ceramic actuator is gradually restored to the initial equilibrium position, and the elastic force generated by the spring is prevented from resetting in transition by the limit nut (3) and the preloading bolt (8).

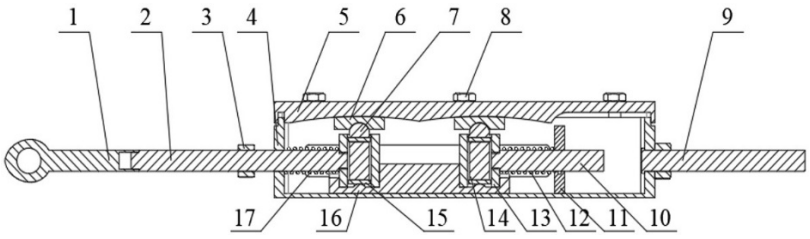

Figure 6 Piezoelectric friction damper construction diagram. Note: 1. pull ring; 2. actuating rod; 3. limit nut; 4. damper shell; 5. curved cover plate; 6. curved friction plate; 7. top tightening terminal; 8. preloading bolt; 9. connecting rod; 10. limit rod; 11. limit plate; 12. self-resetting spring I; 13. actuator sleeve; 14. piezoelectric ceramic actuator; 15. spacer; 16. planar friction plate; 17. self-resetting springs II.

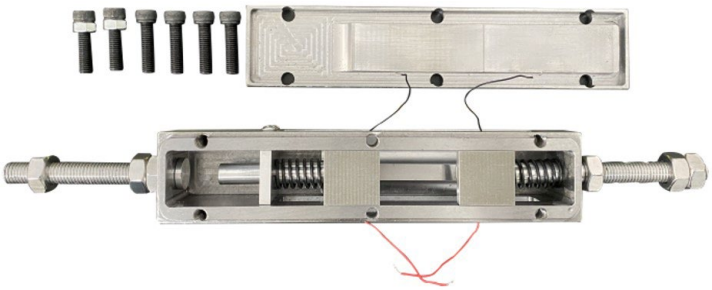

Figure 7 Physical view of piezoelectric friction damper

It is worth noting that, in the process of the piezoelectric ceramic driver being energized and in motion, due to the geometric structural design of the curved cover plate (5) and the curved friction plate (6), an elastic force between the two curved surfaces will be generated additionally, while increasing the positive pressure between the curved cover plate and the curved friction plate and thus increasing the friction damping force generated by the damper, and the curvature of the curved cover plate (5) and the curved friction plate (6) is consistent, so that both can be closely fit together to ensure sufficient friction. Therefore, the design effectively improves the output of the friction damping force compared to the plane friction of a general piezoelectric variable friction damper. In addition, the top tightening terminal (7) and the curved friction plate (6) are in spherical contact, which can ensure the smoothness of the piezoelectric ceramic actuator (14) in the process of horizontal movement; the planar friction plate (16) adopts the two actuator sleeves as a whole solid connection, which can increase the friction area of the planar friction plate and ensure the consistency of the actuator's movement.

In summary, the piezoelectric variable friction damper generates zero displacement thrust by applying a voltage to the piezoelectric ceramic actuator, so that the positive pressure between the piezoelectric ceramic actuator and the damper casing becomes larger, which can achieve the purpose of real-time adjustment of the energy consumption of the damper, so that the damper can realize the intelligent characteristics.

3.2 Damper Output Performance Test and Analysis

Tests were conducted for the output performance of the developed piezoelectric variable friction damper and the test setup is shown in figure 8.

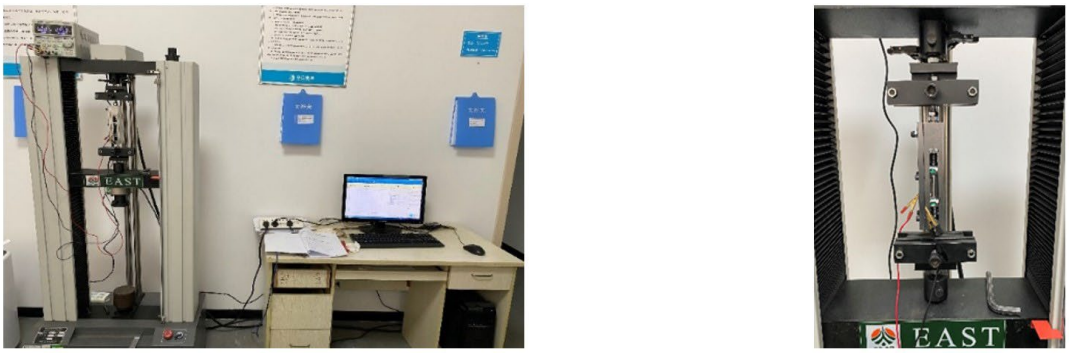

(a) Electronic universal testing machine and control terminal (b) Detailed view of tester clamping

Figure 8 Piezoelectric friction damper performance test equipment

Before the test, the piezoelectric ceramic actuator needs to be adjusted to be located in the initial equilibrium position of the damper, and then the damper is fixed and clamped on the electronic universal testing machine. The computer control terminal is utilized for triangular wave displacement excitation, as shown in figure 9, because the unidirectional travel of the limit bar and the actuator bar in the damper is 0.01 m, the peak value of the triangular wave displacement is set to 0.005 m. Two piezoelectric ceramic actuators are installed in the damper, and the loading voltages are 0 V, 15 V, 30 V, 45 V, and 60 V. The final displacement and damping force are collected by the sensors of the ECTM and fed back to the computer control terminal. magnitude of damping force and feedback to the computer control terminal.

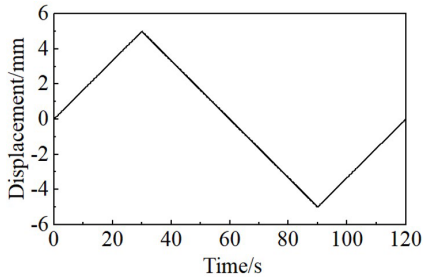

Figure 9 Triangular wave displacement excitation

During the test, due to the damper by the electronic universal testing machine as shown in figure 9 triangular wave displacement excitation, the piezoelectric ceramic actuator in the damper internal motion process can be divided into three stages, as shown in figure 10. Before the start of the test, adjust the piezoelectric ceramic actuator to the initial equilibrium position, at this time the two reset springs are in a natural state, recorded at this time the displacement is 0, as shown in figure 10 (a). With the displacement control loading, the piezoelectric ceramic actuator moves to the set maximum displacement of 5mm, so that the reset spring located on the top is in the state of compression, and the lower spring is in the state of elongation, as shown in figure 10(b), and stipulates that the direction of motion of this section of the 0~30s is the positive direction. In the 30s~90s, the piezoelectric ceramic actuator moved to the maximum displacement in the negative direction, causing the lower reset spring to be in compression, as shown in figure 10(c). Until the 120s, the piezoelectric ceramic actuator motion returns to the equilibrium state, at which the displacement is 0, as shown in figure 10(d).

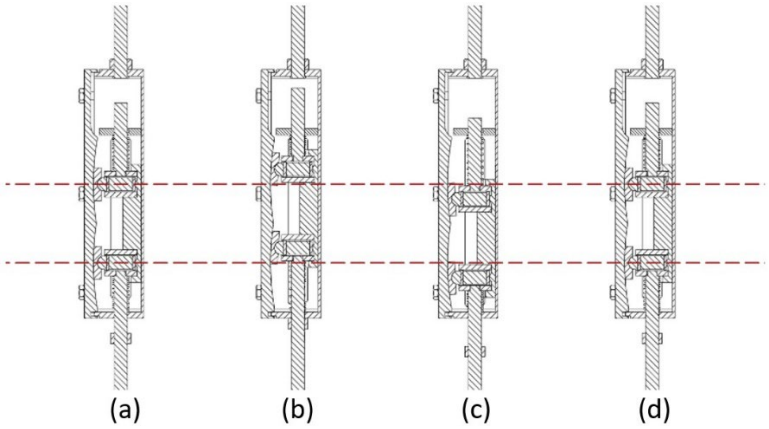

Figure 10 Schematic diagram of the change in motion of the piezoelectric friction damper

Figure 11 shows the displacement-damping force test relationship curve obtained from the test. By calculating the average value of positive and negative damping force at all levels of loading voltage, the relationship curve of test loading voltage-damping force was obtained by applying MATLAB fitting, as shown in figure 12, and the linear relationship was obtained as:

$$f_1 = 16.4835U + 52.9160 \tag{5}$$

In Equation (5), f1 is the damping force of the damper test output.

As can be seen from figure 11, under the same level of voltage, the negative damping force is higher than the positive damping force by 18.07% on average, the reason for this phenomenon is due to the damper in the test process to keep the vertical clamping, when the damper produces a negative damping force, the electronic test universal machine not only has to overcome the damping force produced by the damper to do the work, but also needs to overcome the gravity of the damper itself. When the voltage increases by 15V, the positive and negative damping force increases by 58.64% and 56.68% respectively, which indicates that the increase of the damping force in both directions is more consistent and has a linear growth trend, and at the same time, it can be seen in figure 12 that the test curves have a high degree of overlap with the fitted curves, which indicates that the damping force has a strong linear relationship with the voltage, and that the damping force increases linearly with the loading voltage.

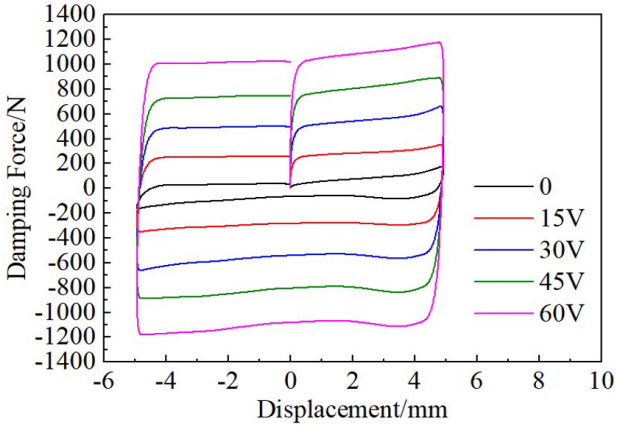

Figure 11 Displacement-damping force test relationship curve

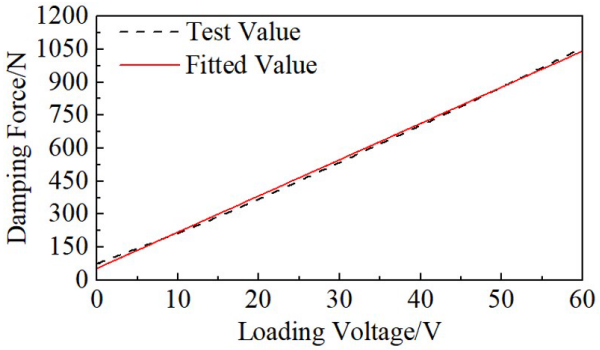

Figure 12 Damper loading voltage-damping force relationship curve

4 PARAMETRIC MODELING BASED ON PIEZOELECTRIC VARIABLE FRICTION DAMPERS

4.1 Mathematical Modeling of Damping Force

The curved cover plate and the curved friction plate in the damper are approximated as two hexahedra as shown in figure 13. The curved cover plate is shown as hexahedron *ABCD*-$A_1B_1C_1D_1$, and the curved friction plate is shown as hexahedron *EFGH*-$E_1F_1G_1H_1$. The two curved surfaces are curved surface $A_1B_1C_1D_1$ and curved surface *EFGH*, respectively, with radii of r = 140 mm, AD = 60 mm, DC = H_1G_1 = 30 mm, AA_1 = 16 mm, E_1H_1 = 40 mm, and EE_1 = 12 mm. According to the working principle of piezoelectric variable friction damper, let the zero-displacement thrust generated by piezoceramic actuator under voltage excitation be F_1, and the curved surface $A_1F_1G_1H_1$ is the curved surface $A_1B_1C_1D_1$. Under the action of F_1, the arc surface $A_1B_1C_1D_1$ is adhered to the arc surface *EFGH*, and when externally disturbed, the actuator rod drives the piezoelectric ceramic actuator to carry out the motion to generate the friction damping force, so that the arc surface friction plate moves along the direction of the arc A_1D_1. The speed of the actuator motion is approximated as a uniform curvilinear motion with a speed of v, such that the elastic force generated between the two arc surfaces is set to F_2.

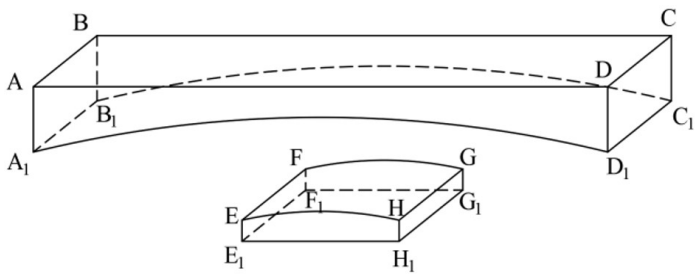

Figure 13 Arc surface friction plate and arc surface cover plate three-dimensional schematic

In the process of motion, according to the theory of elastic mechanics, the deformation energy between two objects can be expressed as:

$$W = \frac{1}{2}\int_V \sigma_{ij}\varepsilon_{ij}dV = \frac{1}{2}\int_{V_1} \sigma_{ij}\varepsilon_{ij}dV + \frac{1}{2}\int_{V_2} \sigma_{ij}\varepsilon_{ij}dV \tag{6}$$

In Equation (6), σ_{ij} is the stress tensor, ε_{ij} is the strain tensor, and $V=V_1+V_2$ is the sum of the volumes of the hexahedron *ABCD-*$A_1B_1C_1D_1$ and the hexahedron *EFGH-*$E_1F_1G_1H_1$.

The two hexahedra can be regarded as elastomers, the applied force F_1 can be regarded as a boundary condition acting on the surfaces of the objects, and the direction of F_1 is approximated as perpendicular to the plane *ABCD*, so the strain tensor between the two contact surfaces is assumed to be:

$$\varepsilon_{ij} = \begin{pmatrix} \frac{1}{r} & 0 & 0 \\ 0 & \frac{1}{r} & 0 \\ 0 & 0 & -\frac{2}{r} \end{pmatrix} \tag{7}$$

In Equation (7), r is the radius of arc $A_1B_1C_1D_1$ and arc *EFGH*.

Since the deformation is elastic, there is a linear relationship between the stress tensor and the strain tensor, which can be expressed as:

$$\sigma_{ij} = C_{ijkl}\varepsilon_{kl} \tag{8}$$

In Equation (8), C_{ijkl} is the elasticity tensor, which contains the elastic properties of the material.

Since the curved friction plate and the curved cover plate are made of the same material, the modulus of elasticity and Poisson's ratio are the same, and both are considered as isotropic materials, the elasticity tensor can be expressed as:

$$C_{ijkl} = \lambda\delta_{ij}\delta_{kl} + \mu\left(\delta_{ik}\delta_{jl} + \delta_{il}\delta_{jk}\right) \tag{9}$$

In Equation (9), λ and μ are Young's modulus and shear modulus, respectively, and δ_{ij} is the Kronecker symbol.

The deformation energy of two more contact surfaces can also be expressed as:

$$W = \frac{1}{2}\int_{V_1+V_2} F_2 x_2 dV \tag{10}$$

In Equation (10), x_2 is the elastic shape variable in the F_2 direction.

Substituting the above equation into the deformation energy equation (6) and solving for F_2 gives:

$$F_2 = \frac{\lambda+3\mu}{r}\left(V_1+V_2\right) + \frac{1}{2}\sqrt{\frac{F_1^2}{\rho^2\left(V_1+V_2\right)^2} + \frac{2v^2}{r^2}} \tag{11}$$

In Equation (11), F_1 and v are the zero-displacement thrust and motion velocity of the piezoelectric ceramic actuator, respectively, and ρ is the density of the material.

Let the positive pressure acting on the piezoelectric ceramic actuator be N, the friction coefficient be μ, and be the relative velocity between the piezoelectric variable friction dampers. Then the damping force model of the piezoelectric variable friction damper (Ou and Yang, 2003) can be expressed as:

$$f = \mu N \operatorname{sgn}\left[\dot{x}\right] \tag{12}$$

In Equation (12), N is related to the pre-tensioning force of the piezoelectric variable friction damper and the adjustable tensioning force generated by the piezoelectric ceramic actuator, as well as the arc elasticity force, i.e:

$$N = \begin{cases} N_0 & E = 0 \\ N_0 + KEd_{33} + F_2 & E > 0 \end{cases} \tag{13}$$

In Equation (13), N_0 is the preload force between the piezoelectric variable friction dampers; K is the shape coefficient, and E is the actively regulated electric field strength of the piezoelectric ceramic actuator, which is related to the input voltage, and K and E are expressed in Equations (14) and (15):

$$K = \frac{n_1 Y_p A_p L_p n_2 Y_l A_l}{n_2 Y_l A_l L_p + n_1 Y_p A_p L_l} \tag{14}$$

$$E = \frac{U}{L_p} \tag{15}$$

In Equations (14) and (15), n_1 and n_2 are the number of piezoelectric ceramic actuators and pretensioned bolts, respectively, Y_p is the modulus of elasticity of the piezoelectric ceramics, A_p is the cross-sectional area of the piezoelectric ceramic actuators, L_p is the axial height of the piezoelectric ceramic actuators, Y_l is the modulus of elasticity of the bolts, A_l is the cross-sectional area of the bolts, L_l is the effective length of the bolts, and U is the loading voltage.

4.2 Parametric Modeling

Modeling the output performance analysis of the damper is the best research method to validate the performance of a piezoelectric ceramic actuator (Pardo-Varela and De la Llera, 2014). In this paper, based on the mathematical model of the damping force of piezoelectric variable friction damper, parametric modeling and analysis are carried out using MATLAB/Simulink. According to the elastic modulus of piezoelectric ceramic $Y_p = 6\times10^6$MPa, the axial height of piezoelectric ceramic actuator $L_p = 0.018$m, the cross-sectional area of piezoelectric ceramic actuator $A_p = 10\times10\times10^{-6}$m^2 = 1×10^{-4}m^2, the effective length of the bolt $L_l = 0.02$m, the elastic modulus of the bolt $Y_l = 2\times10^6$MPa, and the cross-sectional area of the bolt $A_l = \pi\times(2.5\times10^{-3})^2$ m^2= 1.96×10^{-5}m^2, and the encapsulated subsystem A is established by combining equation (14), as shown in figure 14.

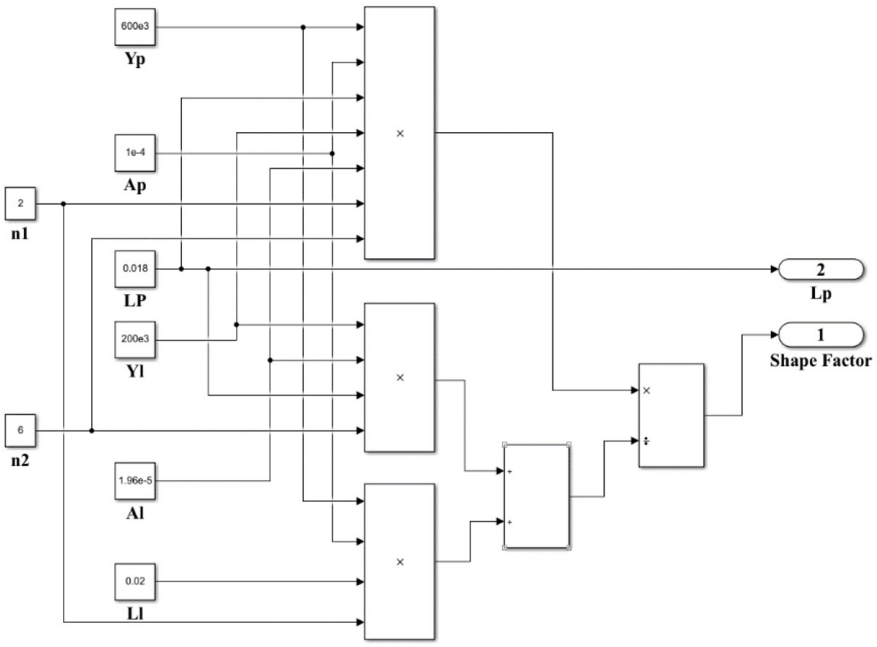

Figure 14 Packaging Subsystem A

From equation (4) loading voltage versus zero displacement thrust, the encapsulated subsystem B is established as shown in figure 15.

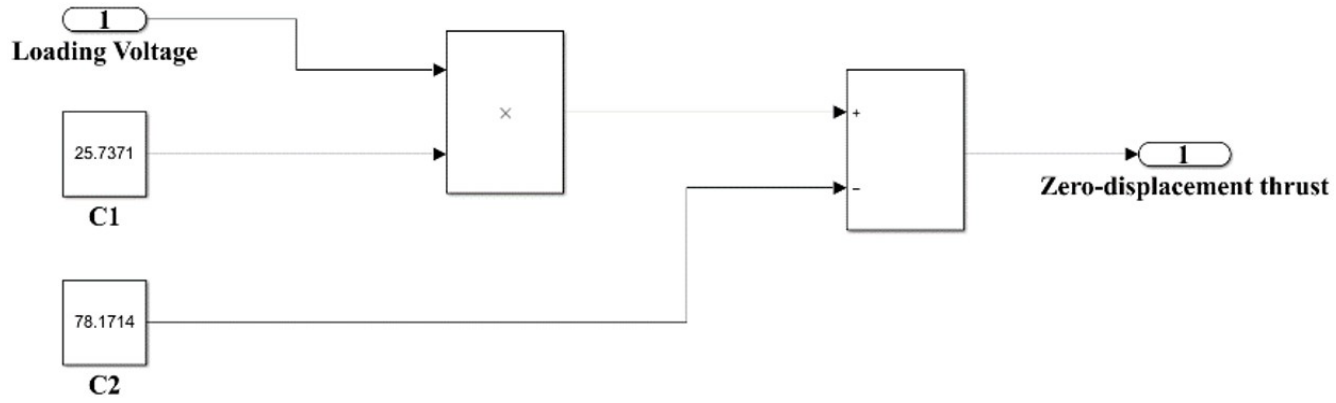

Figure 15 Packaging Subsystem B

Since the material selected for the curved cover plate and the curved friction plate is 45 steel, the density $\rho = 7.85 \times 10^3 kg/m^3$ is taken, so that a, b, c, e, f, and g are AD, DC, AA_1, E_1H_1, H_1G_1, and EE_1 in figure 12, respectively, and the Young's modulus $\lambda = 209 \times 10^6 MPa$ and shear modulus $\mu = 8.23 \times 10^{10} MPa$, and combined with equation (11), the encapsulation subsystem C is established encapsulation subsystem C, as shown in figure 16.

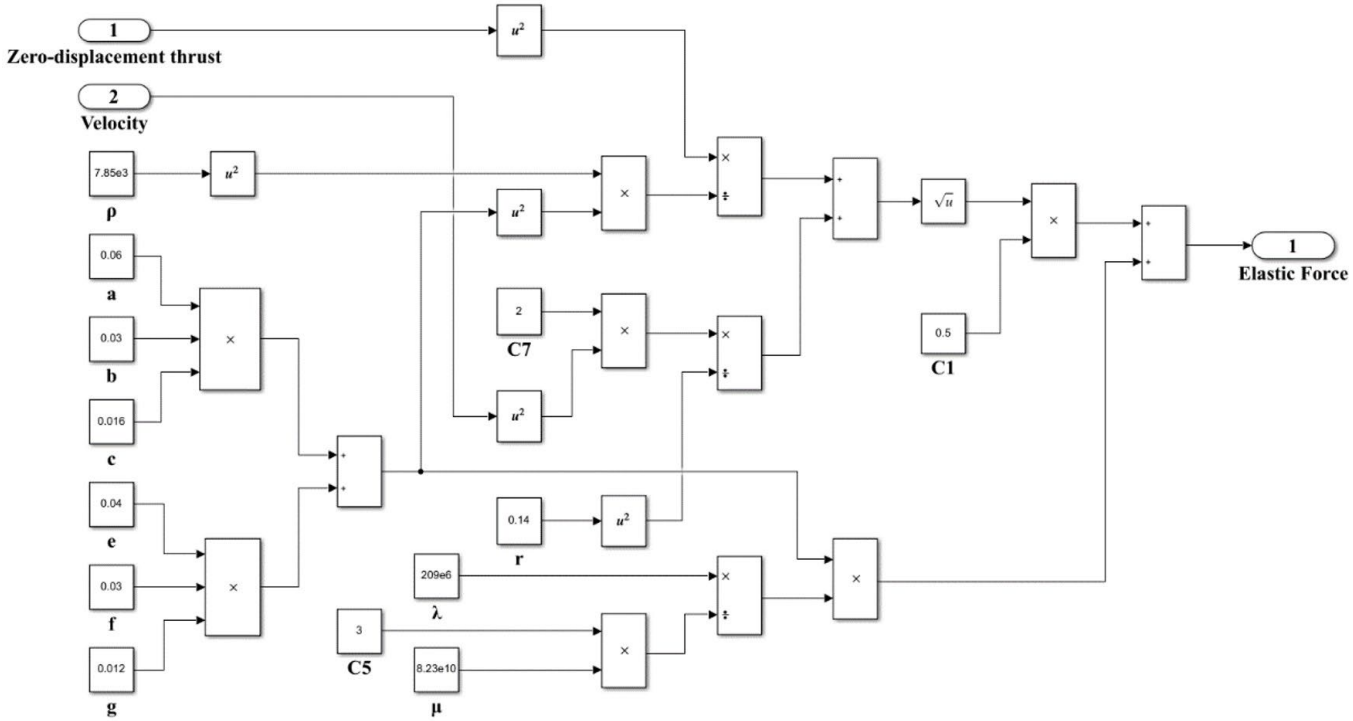

Figure 16 Packaging Subsystem C

From the axial piezoelectric strain constant of piezoelectric ceramics, $d_{33} = 750 \times 10^{-12} m/V$, taking the friction coefficient $\mu_1 = 0.45$, and the preload force of a single preload bolt is 250N, the parametric modeling general diagram is established by combining equations (12), (13) and all the encapsulated sub-systems, with the input variables of the model being the loading voltage and displacement, and the output variable being the damping force as shown in figure 17.

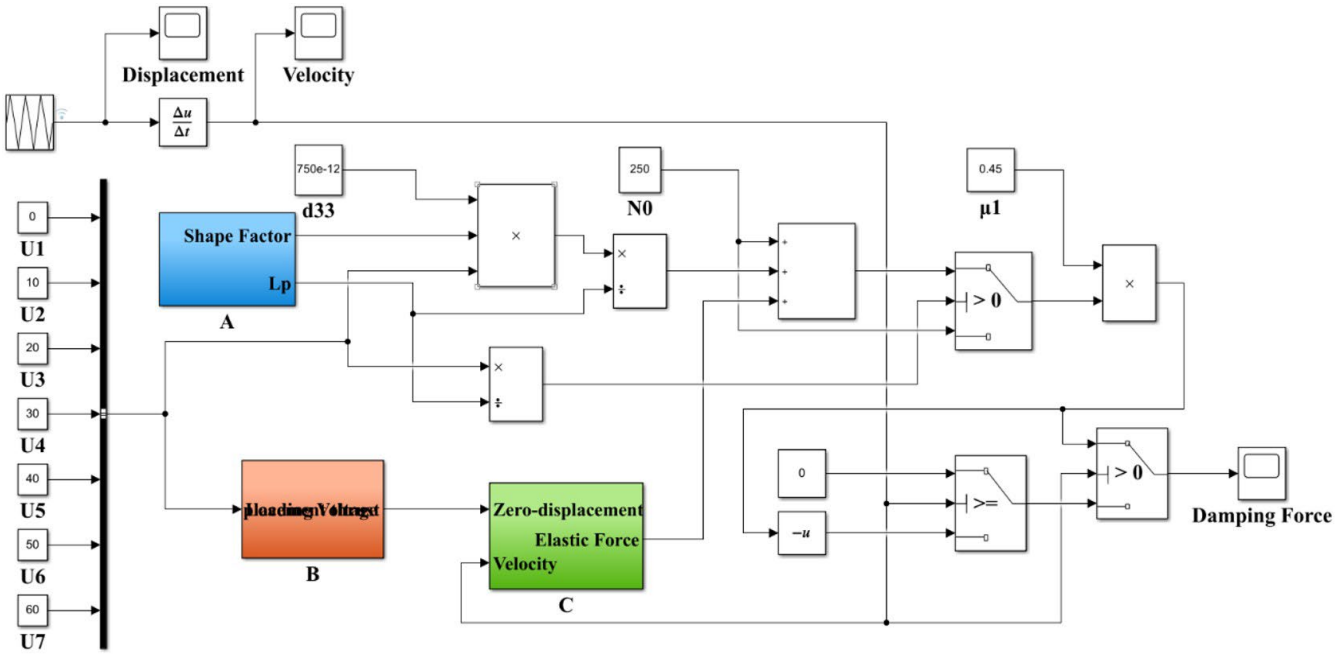

Figure 17 Parametric modeling general diagram

Among them, the displacement input adopts the triangle wave excitation unified with the electronic universal testing machine in the test, and to ensure the complete travel of the piezoelectric ceramic actuator in the damper under the clamping of the electronic universal machine in the simulation test, the sampling time of Simulink is set to 120s.

5 COMPARATIVE ANALYSIS OF DAMPER TESTS AND SIMULATIONS

Extracted simulations are compared with the displacement-damping force relationship for loading voltages of 0, 15V, 30V, 45V, and 60V during the test, as shown in figure 18. Figure 19 shows the numerical simulation relationship curve of velocity-damping force. The average values of the positive and negative damping forces in the test are calculated and compared with the numerical simulation results, as shown in Table 2.

Combined with figure 18 and Table 2, it can be seen that when the loading voltage is 0, the output damping force is 11.25N in simulation, and the output positive and negative damping forces are 63.44N and 87.34N respectively in test, which indicates that the damper can still output a small amount of damping force under the preload force of the pretensioned bolts in the case of no-voltage loading. When the loading voltage increases by 15V, the simulated value of the output damping force increases by 256.14N step by step, and the average test value of the output damping force increases by 259.66N step by step, indicating that the damping force has a linear incremental relationship with the voltage, and the reason for this phenomenon may be due to the linear relationship between the zero-displacement thrust of piezoelectric ceramic actuator and the loading voltage, the elasticity of the reset spring and the linear relationship of the expansion displacement, the friction force generated by the friction plate and the compression force, and the friction force generated by the friction plate and the compression force of the friction plate. Friction generated by the friction plate and the piezoelectric ceramic actuator zero displacement thrust of the linear relationship, the three linear relationship produced a superposition effect. Negative damping force in the test compared to the positive damping force increased by 18.07% on average, the simulation of the two directions of the damping force size is the same, and the loading voltage of 30V, 60V, for example, the test damping force was higher than the simulation of the damping force of 13.89%, 7.6%, this is due to the gravity of the structure of the damper in the test as well as the electronic universal testing machine in the displacement of the loading error can hardly be avoided, and in the numerical simulation This is due to the gravity of the damper structure in the test and the electronic universal testing machine displacement loading error is difficult to avoid, while in the numerical simulation, only the intrinsic properties of the damper and the internal geometric parameters of the influence of the factors, and piezoelectric ceramic zero-displacement thrust and the loading voltage relationship between the function of the longitudinal intercept error, which led to the test results are greater than the simulation.

Combined with figure 18 and figure 19, it can be seen that when the loading voltage is 30V and 60V, for example, the size of the damping force in the simulation is 471.67N and 983.95N to keep the same, and the size of the damping force in the test fluctuates less, with the average value of 537.20N and 1059.18N, which indicates that the size of the damping force is not basically affected by the input displacement and velocity, and the input voltage is the determining factor that affects the size of the damping force. The input voltage is the decisive factor affecting the magnitude of the damping force. When the displacement increases from 0, there is a sudden increase in damping force, followed by a sudden increase in speed, this is due to the piezoelectric ceramic drive from rest to motion will produce a sudden increase in acceleration, resulting in an instantaneous increase in the damping force, which makes the friction plate inside the damper and the shell bottom plate, the curved cover and the curved friction plate to produce sliding friction, resulting in the formation of the piezoelectric ceramic drive speed of the phenomenon of instantaneous increase.

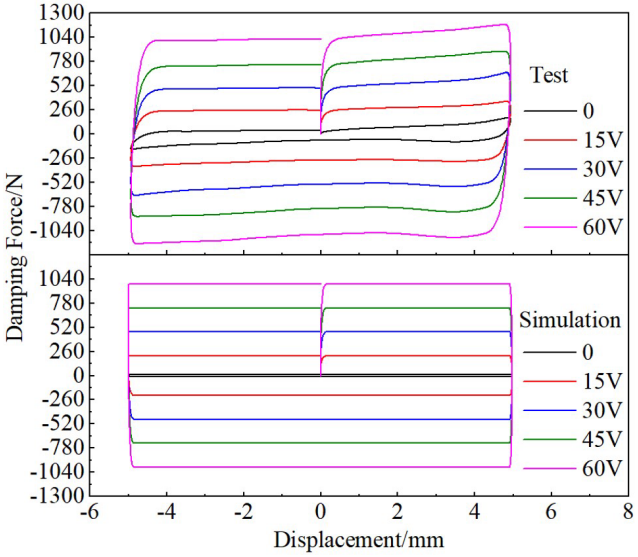

Figure 18 Comparison of displacement-damping force test and simulation relationship curves

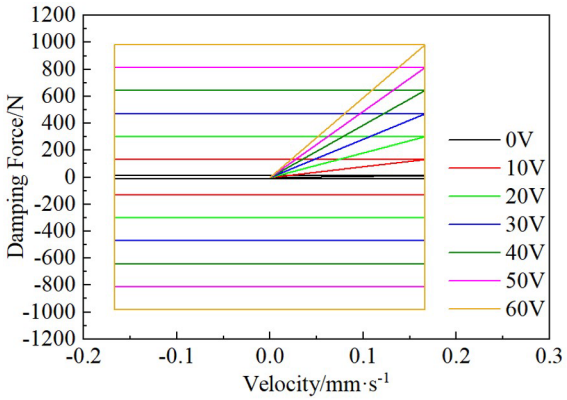

Figure 19 Velocity-damping force simulation relationship curve

Table 2 Comparison of simulated and test output damping force

Loading Voltage /V	Test		Simulation	
	Positive Damping Force /N	Negative Damping Force /N	Positive Damping Force /N	Negative Damping Force /N
0	63.44	-87.34	11.25	-11.25
15	260.58	-299.81	215.53	-215.53
30	501.40	-572.99	471.67	-471.67
45	738.12	-832.19	727.81	-727.81
60	1005.92	-1112.43	983.95	-983.95

Based on the above comparative analysis of test and simulation, MATLAB was used to fit the loading voltage-damping force relationship curve, as shown in figure 20, and the linear relationship was finally obtained as:

$$f = 16.434U + 21.711 \tag{16}$$

In Equation (16), f is the output damping force of the piezoelectric variable friction damper and U is the loading voltage.

From figure 20, the damping force and the loading voltage are linearly increasing with a slope of 16.434, indicating that the test and the simulation show a good agreement of the law, and the loading voltage of the damper is the determining factor of the output damping force.

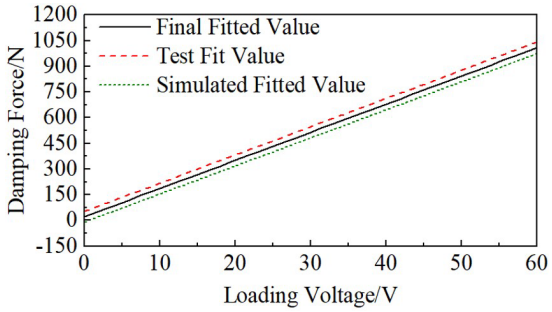

Figure 20 Comparison of fitting curves between loading voltage and damping force

6 CONCLUSION

In this paper, a piezoelectric variable friction damper is developed, the output performance of piezoelectric ceramic actuator and damper is analyzed experimentally, and parametric modeling is carried out based on the mathematical model of the damping force, so as to carry out a comparative analysis between simulation and test, mutually verify the reasonableness of the simulation and the reliability of the test, and arrive at the following conclusions:

1. Through the output performance test of piezoelectric ceramic actuator, it can be obtained that the displacement deformation of the actuator increases with the loading voltage and shows an approximate linear relationship with the magnitude of the loading voltage with a slope of 0.1482; the actuator is mechanically clamped, and the zero-displacement thrust increases with the voltage and shows a strong linear relationship with a slope of 25.7371 in an approximate manner.
2. Through the piezoelectric variable friction damper output performance test can be obtained, the damper in the test process to maintain the vertical clamping, when the damper produces a negative damping force, the electronic test universal machine not only to overcome the damping force produced by the damper to do the work, but also need to overcome the damper's own gravity, resulting in the same level of voltage under the negative damping force is higher than the positive damping force of an average of 18.07%; and when the voltage is increased by 15V each, positive and negative damping force increased by 58.64%, 56.68% respectively, indicating that the increase in both directions is more consistent and has a linear growth trend. When the voltage is increased by 15V, the positive and negative damping forces are increased by 58.64% and 56.68% respectively, which indicates that the increase of the damping force in both directions is more consistent and has a linear growth trend.
3. Through the numerical simulation of the output performance of the piezoelectric variable friction damper, it can be obtained that the damper can still output a small amount of damping force under the preload when the loading voltage is 0. When the loading voltage is increased by 10V every time, the damping force is incremented step by step by 170.76N, which indicates that the damping force is in a linear incremental relationship with the voltage; the magnitude of the damping force is not affected by the input displacement and velocity, and the input voltage is a determining factor affecting the magnitude of the damping force.
4. A comparative analysis of the output performance of the piezoelectric variable friction damper between test and simulation shows that the simulated value of the output damping force increases step by step by 256.14N for every 15V increase in the loading voltage, and the average step by step increase of the test value of the output damping force by 259.66N, which indicates that there is a linearly increasing relationship between the damping force and the voltage, and the slope of the linear increase is 16.434.

Acknowledgments

This project is funded by the Natural Science Foundation of China (52174061; 51808446) and Key Research and Development Program of Shaanxi (2022SF-305), and the Shaanxi Qin Chuang Yuan "Scientist + Engineer" team construction project (2023KXJ-194), and Postgraduate Innovation and Practice Ability Development Fund of Xi'an Shiyou University (YCS23113071).

Author's Contributions: Conceptualization, Jianbo Dai and Zewen Zhao; Methodology, Zewen Zhao and Hao Wang; In-vestigation, Jing Ma and Xuhao Liang; Writing - original draft, Zewen Zhao; Writing - review & editing, Jianbo Dai and Zewen Zhao; Funding acquisition, Jianbo Dai; Resources, Jianbo Dai; Supervision, Jianbo Dai.
Editor: Marcílio Alves

REFERENCES

Liu X. C. (2022). Research on energy dissipation and vibration reduction seismic reinforcement technology of continuous steel bridge bearings, Building Structure, 52(14): 98-102 (in Chinese).

López I., Busturia J.M., Nijmeijer H. (2004). Energy dissipation of a friction damper, Journal of Sound and Vibration, 278(3): 539-561. https://doi.org/10.1016/j.jsv.2003.10.051

Qu J. T., Zhang C., Zhang X., et al. (2023). Experimental study on a new self-centering variable friction damper, China Earthquake Engineering Journal, 45(01): 20-26 (in Chinese).

Jaisee S., Feng Y., Yi H. O., (2021). A state-of-the-art review on passive friction dampers and their applications, Engineering Structures, 235(15). https://doi.org/10.1016/j.engstruct.2021.112022

Yao X. C., Zhao C., Zeng T. (2019). Research Progress and Application Status of Piezoelectric Materials for Vibration Control, Materials for Mechanical Engineering, 43(06): 72-76 (in Chinese).

Li Z. C., Xiong X., Wang H. N., et al. (2023). Research on Composite Control Method of Piezoelectric Actuator, Machinery Design & Manufacture, 384(02): 11-14 (in Chinese).

Padoin E., Fonseca J. S. O., Perondi E. A., et al. (2015). Optimal Placement of Piezoelectric Macro Fiber Composite Patches on Composite Plates for Vibration Suppression, Latin American Journal of Solids and Structures, 12(05): 925-947. http://dx.doi.org/10.1590/1679-78251320

Sokół K., (2020). Passive control of instability regions by means of piezoceramic elements, Latin American Journal of Solids and Structures, Latin American Journal of Solids and Structures, 18(01): 1-12. https://doi.org/10.1590/1679-78256015

Sun L., Li W., Wu Y., et al. (2017). Active vibration control of a conical shell using piezoelectric ceramics, Journal of Low Frequency Noise, Vibration and Active Control, 2017, 36(04): 366-375. https://doi.org/10.1177/146134841774430

Dai N. X., Tan P., Zhou F.L., (2013). Piezoelectric variable friction damper and its performance experiments and analysis, Earthquake Engineering and Engineering Dynamics, 33(03): 205-214 (in Chinese).

Zhu J. Q., Huang M. Q., Li B. X., et al. (2017). Under the action of earthquake, the application of single lay-er shell structure stability dynamic with piezoelectric friction damper, World Earthquake Engineering, 33(02): 135-141 (in Chinese).

Zhan M., Wang S. L., Zhu J. Q., et al. (2015). Vibration control tests of a model structure installed with piezoelectric friction damper with reset function, 34(14): 45-50 (in Chinese).

Wang T., Zhang X., Li K., et al. (2021). Mechanical performance analysis of a piezoelectric ceramic friction damper and research of its semi-active control strategy, Structures, 33: 1510-1531. https://doi.org/10.1016/j.istruc.2021.04.100

Zhang X., Luo Q., Han Q., et al. (2023). Hysteretic be-haviour and structural control performance of a piezo-electric friction damper, Smart Materials and Structures, 2023, 32(01).

Ou J. P., Yang Y. (2003). Piezoelectric-T shape variable friction damper and its performance tests and analysis, Earthquake Engineering and Engineering Dynamics, (04): 171-177 (in Chinese).

Pardo-Varela J., De la Llera J. C. (2014). A Semi-active piezoelectric friction damper, Earthquake Engineering Structural Dynamics, 44(03): 333-354. https://doi.org/10.1002/eqe.2469